Talanta 85 (2011) 493–498

Contents lists available at ScienceDirect

Talanta

journal homepage: www.elsevier.com/locate/talanta

Layer-by-layer assembly of electroactive dye/inorganic matrix film and its application as sensor for ascorbic acid

Xianggui Kong, Wenying Shi, Jingwen Zhao, Min Wei*, Xue Duan

State Key Laboratory of Chemical Resource Engineering, Beijing University of Chemical Technology, Beijing 100029, China

ARTICLE INFO

Article history:
Received 15 December 2010
Received in revised form 7 April 2011
Accepted 10 April 2011
Available online 16 April 2011

Keywords:
Naphthol green B
Layered double hydroxides
Layer-by-layer
Ultrathin films
Electrocatalysis

ABSTRACT

A novel inorganic–organic composite ultrathin film was fabricated by layer-by-layer assembly of naphthol green B (NGB) and layered double hydroxides (LDHs) nanoplatelets, which shows remarkable electrocatalytic behavior for oxidation of ascorbic acid. LDHs nanoplatelets were prepared using a method involving separate nucleation and aging steps (particle size: 25 ± 5 nm; aspect ratio: 2–4) and used as building blocks for alternate deposition with NGB on indium tin oxide (ITO) substrates. UV–vis absorption spectroscopy and XRD display regular and uniform growth of the NGB/LDHs ultrathin film with extremely *c*-orientation of LDHs nanoplatelets (*ab* plane of microcrystals parallel to substrates). A continuous and uniform surface morphology was observed by SEM and AFM image. The film modified electrode displays a couple of well-defined reversible redox peaks attributed to Fe^{2+}/Fe^{3+} in NGB ($\Delta E_p = 68$ mV and $I_a/I_c = 1.1$). Moreover, the modified electrode shows a high electrocatalytic activity towards ascorbic acid in the range 1.2–55.2 μM with a detection limit of 0.51 μM (S/N = 3). The Michaelis–Menten constant was calculated to be $K_M^{app} = 67.5$ μM.

1. Introduction

Ascorbic acid (AA) plays a key role in participating several biological reactions and preventing many diseases including mental illness, infertility and cancer, as a result various techniques have been employed for its detection [1–3]. Electrochemical sensors have attracted much attention among these analytical tools due to their excellent sensitivity, rapid response, low cost and well convenience [4–6]. However, the electrochemical reaction of AA at bare electrodes is irreversible with poor sensitivity and selectivity; therefore, considerable interest has been focused on modified electrodes with redox enzymes owing to their high selectivity and activity [7,8]. Unfortunately, it is difficult to attain an efficient electron transfer between enzyme and electrode since the electroactive centers are usually embedded within the macromolecule. Therefore, considerable attention has been paid to develop nonenzymatic electrodes to solve this problem.

Naphthol green B (NGB, Fig. 1A), a kind of small molecule dye, has been widely used as electroactive material owing to its high electron transfer efficiency in electrocatalysis reaction [9,10]. However, its long-term stability, toxicity and pollution remain unresolved in practical applications. Inorganic nanoparticles, owing to their small size, unique chemical, physical and electronic properties that are different from those of bulk materials, have been applied as electron transfer mediator or carrier for electroactive substance in chemically modified electrodes [11–13]. Therefore, the incorporation of electroactive organic species within inorganic matrix can be an effective solution for the purpose of obtaining durable solid electrochemical sensors with high stability as well as repeatability.

Layered double hydroxides (LDHs), also known as hydrotalcites or anionic clays, are a class of naturally occurring and synthetic materials, which can be described by the general formula $[M^{II}_{1-x}M^{III}_x(OH)_2]^{z+}(A^{n-})_{z/n}\cdot yH_2O$ (M^{II} and M^{III} are divalent and trivalent metals respectively; A^{n-} is the interlayer anion compensating for the positive charge of the metal hydroxide layers). Based on the 2D-organized structure, flexibility in composition and unique ion-exchange property, LDHs materials have shown a wide variety of potential applications in catalysis, electrochemistry, medicine and environmental remediation [14–16]. Furthermore, compared with other inorganic materials, LDHs exhibit many advantages: nanoplatelet crystallinity, easy control of particle size, high stability and biocompatibility. These intrinsic properties provide a suitable microenvironment for the immobilization of electroactive substances and accelerate the direct electron transfer between redox species and the underlying electrode [17,18].

In this work, a novel ultrathin film was fabricated by alternate assembly of NGB and LDHs nanoplatelets on indium tin oxide (ITO) electrode *via* the layer-by-layer (LBL) method [19–21], which shows a good electrocatalytic activity for the oxidation of AA. The ultrathin film exhibits an ordered architecture at the nanometer level, whose thickness and composition sequence can be con-

* Corresponding author. Tel.: +86 10 64412131; fax: +86 10 64425385.
E-mail addresses: weimin-hewei@163.com, weimin@mail.buct.edu.cn (M. Wei).

0039-9140/$ – see front matter © 2011 Elsevier B.V. All rights reserved.
doi:10.1016/j.talanta.2011.04.020

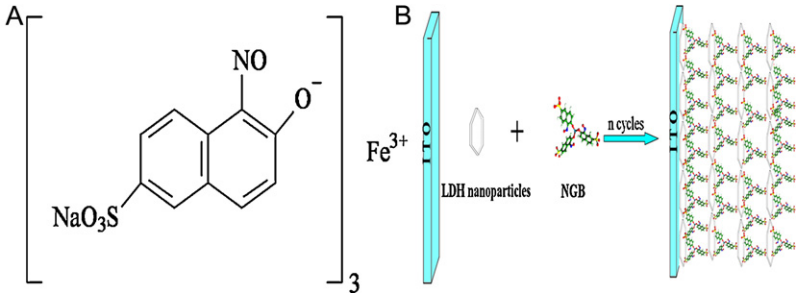

Fig. 1. (A) Chemical structure of NGB and (B) assembly process for the $(NGB/LDHs)_n$ multilayer film.

trolled precisely. The electrochemical behavior of the NGB/LDHs film attributed to Fe^{2+}/Fe^{3+} in NGB was obtained ($\Delta E_p = 68$ mV and $I_a/I_c = 1.1$), owing to the high dispersion and uniform arrangement of NGB molecules within the LDHs matrix. In addition, the NGB/LDHs film modified electrode exhibits excellent electrocatalytic performance for AA with a low detection limit, high sensitivity and stability as well as good selectivity in the presence of interfering compounds. Therefore, this work demonstrates a successful paradigm for the fabrication of ultrathin films based on organic electroactive species and inorganic nanoplatelets, which can be potentially applied in electrocatalysis and electrochemical sensor.

2. Experimental

2.1. Reagents and materials

Naphthol green B (NGB) was purchased from Alfa Aesar Chemical Co. Ltd. All other chemicals were of analytical grade and used without further purification. All the solutions were prepared using water purified in a Milli-Q Millipore system (>18 MΩ cm).

2.2. Fabrication of the NGB/LDHs nanoplatelets film modified electrode

The colloidal suspension of Ni-Al LDHs nanoplatelets was prepared by the method developed by our group [22,23]. The multilayer films of NGB/LDHs were fabricated by applying the LBL method. Briefly, the substrate (ITO) was firstly dipped into the colloidal LDHs suspension (0.6 g/L) for 10 min followed by rinsing with deionized water thoroughly, and then immersed into a solution of NGB (1.0 g/L) for 10 min and washed extensively. Subsequently, a series of these operations for LDHs nanoplatelets and NGB were repeated n times to obtain multilayer films of $(NGB/LDHs)_n$ (Fig. 1B). The resulting films were dried with nitrogen gas flow. All experiments were performed at room temperature.

2.3. Characterization techniques

Powder XRD patterns were recorded by a Shimadzu XRD-6000 diffractometer, using Cu Kα radiation ($\lambda = 0.15418$ nm) at 40 kV, 30 mA. UV–vis spectra were collected on a Shimadzu U-3000 spectrophotometer. The morphology of thin films was investigated using a scanning electron microscope (SEM Hitachi S-4700) with the accelerating voltage of 20 kV. The surface roughness was studied using the atomic force microscopy (AFM) software (Digital Instruments, Version 6.12). The electrochemical measurements were performed using a CHI 660C electrochemical workstation (working electrode: modified ITO; auxiliary electrode: a platinum foil; reference electrode: KCl saturated Ag/AgCl electrode). Electrochemical impedance spectroscopy (EIS) measurements were performed on $(NGB/LDH)_n$ modified electrodes in 0.1 M KCl with 5 mM $Fe(CN)_6^{3-/4-}$ solution at a potential of +0.22 V *vs.* Ag/AgCl. The EIS dispersions were recorded in the frequency range 0.01–100 kHz. A 0.1 M phosphate buffer solution (PBS, pH = 7.5) was used as electrolyte that saturated by N_2 in advance. All measurements were performed at room temperature.

3. Results and discussion

3.1. Characterization of the ultrathin films

The Ni/Al-LDHs nanoplatelets were prepared by a method involving separate nucleation and aging steps developed by our

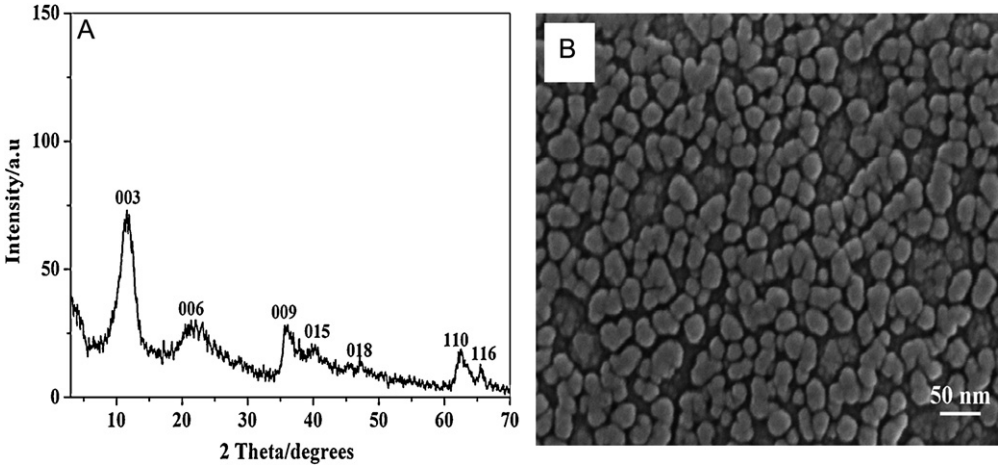

Fig. 2. (A) XRD pattern and (B) SEM image of the Ni/Al-LDHs nanoplatelets.

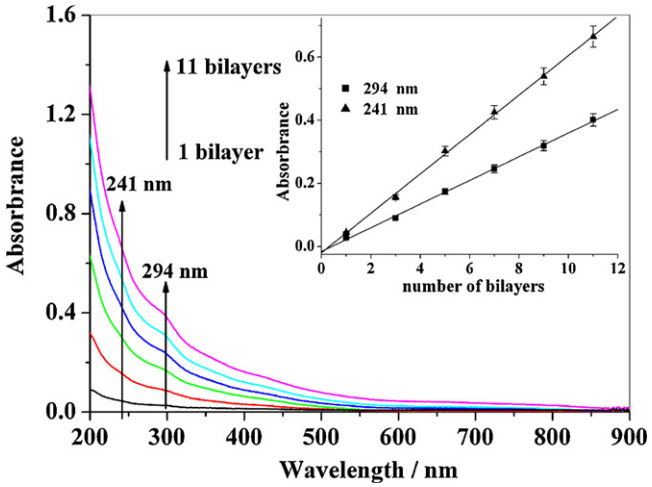

Fig. 3. UV–vis absorption spectra of the $(NGB/LDHs)_n$ films (n = 1–11) on quartz glass substrates. Inset displays the plots of absorbance of the multilayer films at 241 and 294 nm *vs.* n.

group [22,23], whose XRD pattern is shown in Fig. 2A. All the reflections can be indexed to a typical hydrotalcite-like structure (Joint Committee on Powder Diffraction Standards file No. 48-0594). Fig. 2B exhibits the SEM image of the obtained LDHs nanoplatelets with round-like shape and narrow particle size distribution (particle size: 25 ± 5 nm; aspect ratio: 2–4), which is favorable for the assembly of uniform ultrathin films. The subsequent growth of the NGB/LDHs multilayer film was monitored by means of the UV–vis absorption band at 241 and 294 nm attributed to the $\pi-\pi^*$ transition in the naphthoquinone structure of NGB (Fig. 3). Compared with the pristine NGB in aqueous solution (235 and 283 nm, Fig. S1), a red-shift for the multilayer film was observed, as a result of the interactions between individual molecules in the densely packed films. The intensity of the absorption bands at 241 and 294 nm correlates nearly linearly with the increase of bilayer number n (Fig. 3, inset), indicating a stepwise and regular deposition of $(NGB/LDHs)_n$ multilayer films.

Successful fabrication of the ultrathin film was further confirmed by XRD patterns (Fig. 4A: the broad reflection in the 2θ range 20–30° is due to the scattering of the substrate). The as-prepared $(NGB/LDHs)_n$ films display a characteristic 003 reflection of CO_3-type LDHs with a basal spacing of 0.78 nm, whose intensity increases gradually upon increasing the bilayer number. Furthermore, reflections (h, $k \neq 0$) at high angle were not observed, indicating a well c-oriented assembly of LDHs nanoplatelets in the film [24]. SEM images (Fig. 4B and C) show that the LDHs nanoplatelets are stacked with *ab*-plane parallel to the substrate, consistent with the XRD results in Fig. 4A. The film is continuous and uniform with an average increment of ~8.3 nm per deposition cycle, which is obtained from the slope of film thickness *vs.* bilayer number (inset in Fig. 4C and Fig. S2). The AFM image (5 μm × 5 μm) of the $(NGB/LDHs)_{10}$ film is shown in Fig. 4D. The average root-mean-square (rms) roughness for the ultrathin films increases slowly from 14.2 nm (n = 5) to 20.9 nm (n = 20) (Fig. S3), indicating a relatively smooth surface of the films.

3.2. Electrocatalytic performance of the ultrathin film

The direct electrochemistry behavior of the modified electrode was investigated in PBS solution (pH 7.5) by cyclic voltammetry (Fig. 5A). Compared with the bare ITO and LDHs nanoplatelets modified ITO electrode, a pair of well-defined and reversible peaks located at 0.632 and 0.564 V (ΔE_p = 68 mV and I_a/I_c = 1.1) were observed for the $(NGB/LDHs)_4$/ITO electrode, which can be ascribed to the reversible one-electron redox reaction of the Fe^{III}/Fe^{II} couple in NGB ($\Delta E^{\theta'}$ = 0.598 V)

$$Fe^{III} - NGB + e \Leftrightarrow Fe^{II} - NGB \quad (1)$$

Moreover, the electroactivity of NGB in solution was investigated as well (Fig. S4). No CV behavior of NGB at a bared ITO was found and a pair of irreversible peaks were observed at the LDHs/ITO electrode. Compared with the CVs of $(NGB/LDHs)_4$/ITO electrode (Fig. 5A), it is concluded that the LDHs matrix effectively immobilizes the NGB molecules in the $(NGB/LDHs)_4$/ITO electrode and accelerates the electron transfer between NGB and electrode surface. Furthermore, for the $(NGB/LDHs)_n$/ITO modified electrode, the peak current increases firstly with the deposition cycles up to 4 bilayers (Fig. 5A, inset d), which is attributed to the enhancement of NGB content; while it decreases from 4 to 6 bilayers due to the increase in the resistance of multilayer films [25] (Fig. 5A, inset e). In addition, the peak potential (ΔE_p) increases in the whole range from n = 1 to n = 6, as a result of the increase in the film resistance (see below Fig. S5) which limits the electron transfer between NGB and electrode surface. Considering the peak current and the peak potential, the $(NGB/LDHs)_4$/ITO was chosen as the working electrode in this work. Fig. S5 displays the electrochemical impedance spectroscopy (EIS) of the electrodes modified by ultrathin films with different bilayers (n = 1–6), demonstrating the impedance changes of the electrode surface during the fabrication process. It was found that the diameter of the Nyquist circle increased linearly along with the bilayer number n (Fig. S5: inset), indicating a successful LBL growth of the $(NGB/LDHs)_n$ ultrathin film on the surface of ITO with almost the same amount of NGB in each cycle. The effect of pH on the electrochemical behavior of the $(NGB/LDHs)_4$/ITO electrode was studied in the range from pH = 6.5 to 8.5 (Fig. 5B). The results show that the peak potential is nearly independent on the pH value, indicating that no proton but electron is involved in the redox process. This further verifies the electrode reaction described in Eq. (1). Taking into account the feasibility and versatility of a physiological environment, the PBS solution (pH = 7.5) was selected as the electrolyte in this work.

Fig. 6A displays the effect of scan rate on the electrochemical response of the $(NGB/LDHs)_4$/ITO. It was found that both anodic and cathodic peak current increased linearly with the increase of scan rate from 0.02 to 0.16 V s^{-1}, suggesting the redox reaction is a surface-controlled electrochemical process. Based on Laviron theory [26,27], if the value of $n\Delta E_p$ > 200 mV, the electron transfer rate constant (k_s) and charge transfer coefficient (α) can be determined by the following equations:

$$\Delta Ep = \Delta E^{\theta'} - 2.303\left(\frac{RT}{\alpha nF}\right)\log(\nu) \quad (2)$$

$$\log k_s = \alpha\log(1-\alpha) + (1-\alpha)\log\alpha - \log\frac{RT}{nF\nu} - \frac{nF\Delta E_p\alpha(1-\alpha)}{2.303RT} \quad (3)$$

where α is the charge transfer coefficient; k_s is the electron transfer rate constant; ν is the scan rate; n is the number of transferred electron; R is the gas constant; F is the Faraday constant; T is the absolute temperature; $\Delta E^{\theta'}$ is the apparent formal potential. According to the linear relationship between E_p and $\log\nu$ (Fig. S6), it was calculated that α = 0.44 and k_s = 3.5 s^{-1} for the $(NGB/LDHs)_4$ ultrathin film modified electrode. The large value of electron transfer rate constant is indicative of high capability of LDHs nanoplatelets for promoting electron between NGB and the electrode surface. In addition, the stability of the $(NGB/LDHs)_4$/ITO was evaluated by consecutive voltammetric sweep method (Fig. 6B). After 200 consecutive cycles, the anodic and catholic current decreased by 3.8% and 2.6% respectively, indicating an excellent stability of the $(NGB/LDHs)_4$ modified electrode.

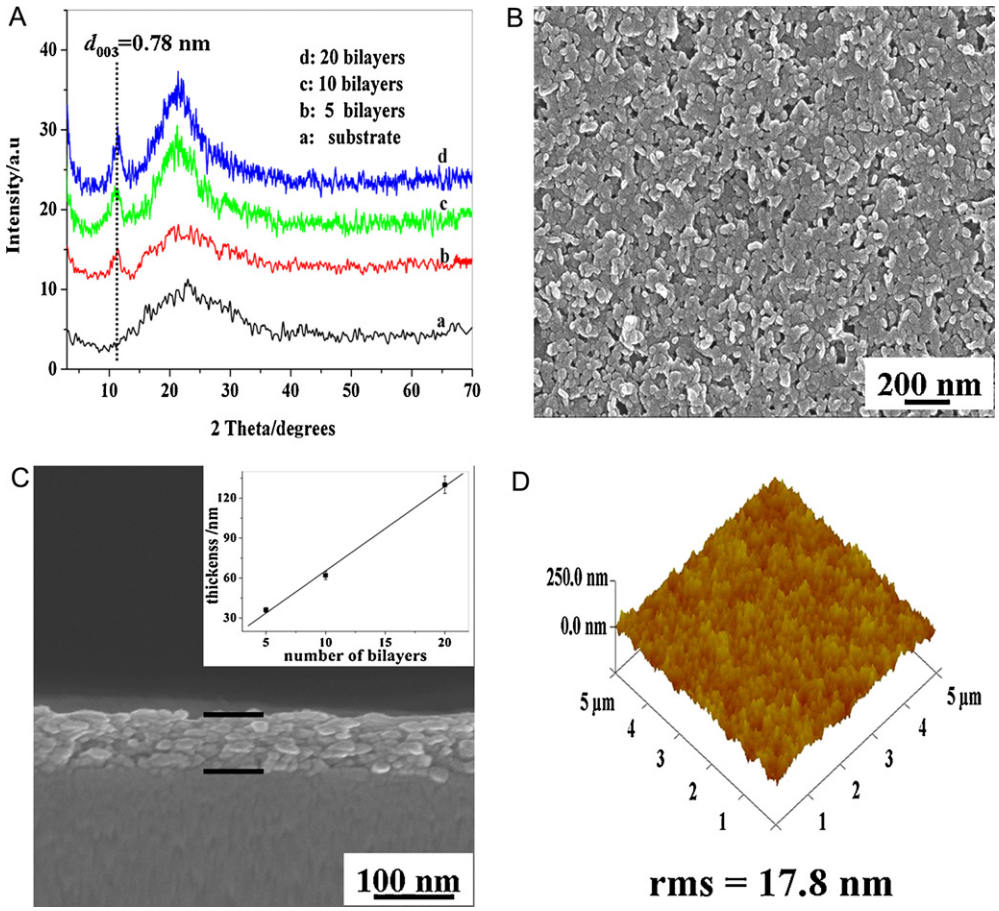

Fig. 4. (A) XRD patterns of the $(NGB/LDHs)_n$ films deposited on quartz glass substrates, (B) top view, (C) cross-sectional SEM image of the $(NGB/LDHs)_{10}$ film; inset of C: plot of film thickness *vs.* bilayer number *n* and (D) tapping-mode AFM image of the $(NGB/LDHs)_{10}$ film.

To verify the advantage of the modified electrode for the AA oxidation, several comparison studies were carried out. Figs. S7 and S8 display the CVs of AA at a bare ITO, at the LDHs/ITO electrode in PBS solution (pH = 7.5) and NGB solution (2 μM) respectively, displaying a poor electrocatalytic activity with low sensitivity and large overpotential of AA oxidation under the identical conditions. Fig. 7 exhibits the electrocatalytic behavior of the $(NGB/LDHs)_4$/ITO electrode for the oxidation of AA. The anodic peak current enhances linearly along with the increase of AA concentration. The linear response ranges in 1.2–55.2 μM with a regression equation of i_{pa} (μA) = 3.9 + 1.1 *C* (10^{-6} M), r^2 = 0.998, and a detection limit of 0.51 μM for AA was obtained based on S/N = 3 (Fig. 7, inset a). The detection limit in this work is lower than that of the $(NGB/PPy)_n$ organic–organic film modified electrode, the carbon fiber microelectrode and the ascorbate oxidase biosensor [28–30]. It's known that the Michaelis–Mentel model was initially proposed to account

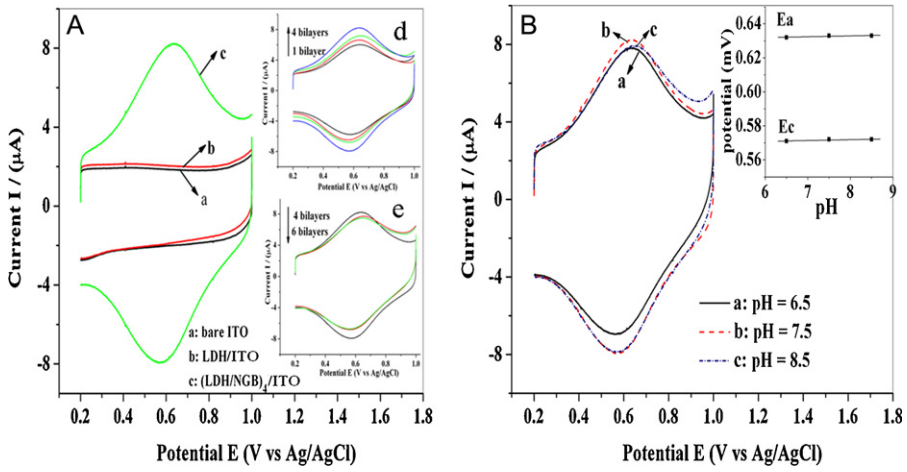

Fig. 5. (A) CVs of (a) a bare ITO, (b) the LDHs nanoplatelets/ITO and (c) the $(NGB/LDHs)_4$/ITO in PBS (pH 7.5) at 0.1 V s^{-1}; the inset d and e display the CVs of $(NGB/LDHs)_n$/ITO with different bilayer number (n = 1–4 and n = 4–6 respectively) and (B) CVs of the $(NGB/LDHs)_4$/ITO in PBS with pH = 6.5, 7.5 and 8.5 respectively at 0.1 V s^{-1}. The inset shows the variation of E_{pa} and E_{pc} as a function of pH value.

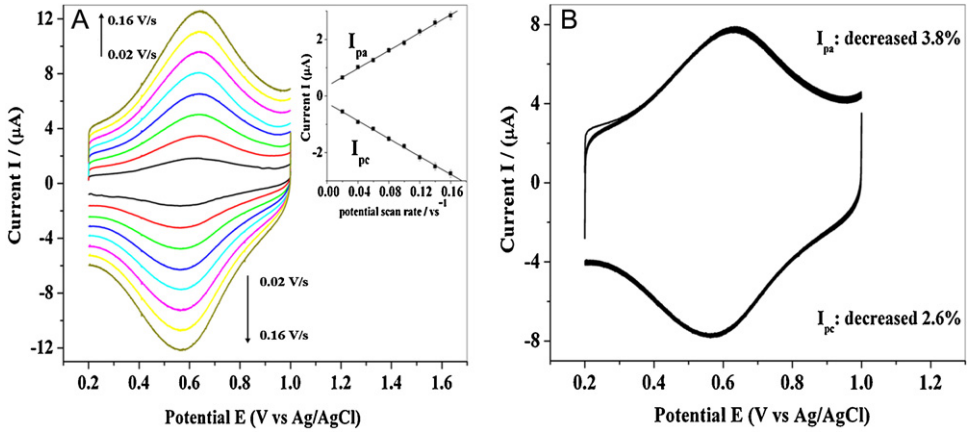

Fig. 6. (A) CVs of the $(NGB/LDHs)_4$/ITO with scan rate ranging from 0.02 to 0.16 V s^{-1} in PBS (pH 7.5); inset: plots of peak current *vs.* scan rate and (B) the stability of the $(NGB/LDHs)_4$/ITO in PBS (pH 7.5) at 0.1 V s^{-1} for 200 consecutive cycles.

for the enzyme kinetics; subsequently, this model was gradually accepted as a fundamental method for many catalysis systems besides enzymatic reactions [31–33]. Herein, a stimulant constant was used to evaluate the electrocatalytic activity of NGB for AA. The Michaelis–Menten constant K_M^{app} can be calculated from the Lineweaver–Burk equation:

$$\frac{1}{I_{ss}} = \frac{1}{I_{\max}} + \frac{K_M^{app}}{I_{\max} C} \quad (4)$$

I_{ss} is the steady-state current after addition of AA, $I_{\max}$ is the maximum current measured under saturated condition and C is the AA concentration. Based on the slope and intercept of the linear correlation between the reciprocals of I_{ss} and C (Fig. 7, inset b), the apparent K_M^{app} was calculated to be 67.5 μM for the $(NGB/LDHs)_4$ electrode. This value is smaller than that of the reported biosensors modified by ascorbate oxidase (157 μM and 166 μM respectively) [29,34], indicating the $(NGB/LDHs)_4$/ITO electrode exhibits a high electrocatalytic activity for AA. Furthermore, hydrogen peroxide, dopamine, uric acid and glucose as interferences were investigated under the same conditions, and the results showed that the percent recovery of the modified electrode was 101.7%, 101.3%, 100.8% and 100.5% respectively for the measurement of AA (10 μM) with 5 times concentration of the interferences, demonstrating the good selectivity to AA for the modified electrode. Moreover, eight replicate measurements of 10 μM AA on one modified electrode yielded a reproducible current with the relative standard deviation (R.S.D.) of 2.6%; additionally, five independent modified electrodes were prepared using the same procedure and used for the determination of AA (10 μM) with the R.S.D. of 2.1%, demonstrating the good repeatability and reproducibility of the electrochemical sensor. The long-term stability was investigated by measuring the current response of 10 μM AA after one month and the percent recovery was 96.8%, indicating the long lifetime stability of the modified electrode. To evaluate the ability of the modified electrode for practical analysis, the proposed sensor was applied to determine AA in three normal human urine samples by utilizing standard addition method (10, 20 and 40 μM, respectively; pH = 7.5, adjusted by dilute HCl). The determined value was 10.5, 20.9 and 41.3 μM for the three samples, and the percent recovery was 105%, 104.5% and 103.3% respectively. This demonstrates that the modified electrode in this work can be used for the detection of AA in biological samples.

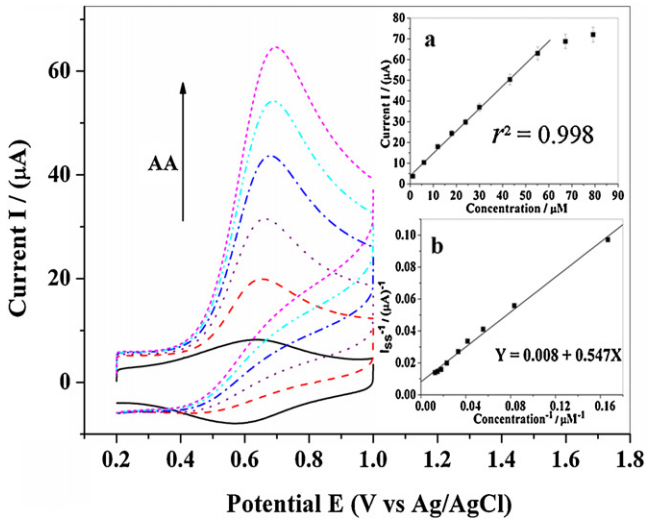

Fig. 7. CVs of the $(NGB/LDHs)_4$/ITO electrode with different concentration of AA at a scan rate of 0.1 V s^{-1}; inset a: the linear relationship between the anodic peak current and concentration of AA; inset b: the Lineweaver–Burk plot for the response of $(NGB/LDHs)_4$/ITO electrode towards AA.

The excellent electrocatalytic performance of the modified electrode indicates that LDHs nanoplatelets provide a favorable microenvironment for facilitating the electron transfer between NGB and electrode surface which could be used as good candidates for the fabrication of reagentless electrochemical sensors. Additionally, the NGB molecules are immobilized in the film *via* LBL approach with high dispersion and uniform arrangement, accounting for the enhancement of electron transfer.

4. Conclusions

In summary, a highly sensitive AA electrochemical sensor has been fabricated based on the alternate assembly of NGB molecules with LDHs nanoplatelets *via* the LBL technique. Structural characterizations show that the well-ordered $(NGB/LDHs)_n$ film is continuous and uniform. The $(NGB/LDHs)_4$ ultrathin film modified electrode exhibits an excellent electrocatalytic activity for the oxidation of AA with high sensitivity, anti-interference and long-term stability. Hence, this work provides a facile and efficient strategy for the immobilization of organic dyes into an inorganic nanoplatelets matrix, for the purpose of potential applications in electroanalysis and electrochemical sensor.

Acknowledgments

This project was supported by the National Natural Science Foundation of China, the 111 Project (Grant No. B07004) and the

973 Program (Grant No. 2011CBA00504) the Collaborative Project from the Beijing Education Committee.

Appendix A. Supplementary data

Supplementary data associated with this article can be found, in the online version, at doi:10.1016/j.talanta.2011.04.020.

References

[1] P. Janda, J. Weber, L. Dunsch, A.B.P. Lever, Anal. Chem. 68 (1996) 960–965.
[2] A. Salimi, H. Mamkhezri, R. Hallaj, Talanta 70 (2006) 823–832.
[3] E.A. Khudaish, A.A.A. Farsi, Talanta 80 (2010) 1919–1925.
[4] M.S. Alaejos, F.J.G. Montelongo, Chem. Rev. 104 (2004) 3239–3266.
[5] L.D. Mello, L.T. Kubota, Talanta 72 (2007) 335–348.
[6] R.F. Carvalhal, M.S. Kfouri, M.H.O. Piazetta, A.L. Gobbi, L.T. Kubota, Anal. Chem. 82 (2010) 1162–1165.
[7] X.Y. Wang, H. Watanabe, S. Uchiyama, Talanta 74 (2008) 1681–1685.
[8] E. Akyilmaz, E. Dinçkaya, Talanta 50 (1999) 87–93.
[9] X.G. Kong, J.W. Zhao, J.B. Han, D.Y. Zhang, M. Wei, X. Duan, Electrochim. Acta 56 (2011) 1123–1129.
[10] Z.Q. Zhang, L.J. Gao, H.Y. Zhan, Talanta 47 (1998) 497–501.
[11] A. Lesniewski, M. Paszewski, M. Opallo, Electrochem. Commun. 12 (2010) 435–437.
[12] E.V. Milsom, H.A. Dash, A.T.A. Jenkins, M. Opallo, F. Marken, Bioelectrochemistry 72 (2008) 1–2.
[13] Z. Dai, A.N. Kawde, Y. Xiang, J.T.L. Belle, J. Gerlach, V.P. Bhavanandan, L. Joshi, J. Wang, J. Am. Chem. Soc. 128 (2006) 10018–10019.
[14] A.M. Fogg, V.M. Green, H.G. Harvey, D. O'Hare, Adv. Mater. 11 (1999) 1466–1469.
[15] A.I. Khan, L.X. Lei, A.J. Norquist, D. O'Hare, Chem. Commun. (2001) 2342–2343.
[16] F. Leroux, A. Illaik, V. Verney, J. Colloid. Interf. Sci. 332 (2009) 327–335.
[17] X.G. Kong, X.Y. Rao, J.B. Han, M. Wei, X. Duan, Biosens. Bioelectron. 26 (2010) 549–554.
[18] X. Chen, C.L. Fu, Y. Wang, W.S. Yang, D.G. Evans, Biosens. Bioelectron. 24 (2008) 356–361.
[19] M. Zhang, K. Gong, H. Zhang, L. Mao, Biosens. Bioelectron. 20 (2005) 1270–1276.
[20] M. Yang, Y. Yang, H. Yang, G. Shen, Biomaterials 27 (2006) 246–255.
[21] H. Zhao, H. Ju, Anal. Biochem. 350 (2006) 138–144.
[22] Y. Zhao, F. Li, R. Zhao, D.G. Evans, X. Duan, Chem. Mater. 14 (2002) 4286–4291.
[23] J.B. Han, Y.B. Dou, M. Wei, D.G. Evans, X. Duan, Angew Chem. Int. Ed. 49 (2010) 2171–2174.
[24] J.A. Gursky, S.D. Blough, C. Luna, C. Gomez, A.N. Luevano, E.A. Gardner, J. Am. Chem. Soc. 128 (2006) 8376–8377.
[25] J. Xu, C. Shi, H. Chen, Langmuir 21 (2005) 9630–9634.
[26] A. Salimi, H. Mamkhezri, R. Hallaj, S. Zandi, Electrochim. Acta 52 (2007) 6097–6105.
[27] E. Laviron, J. Electroanal. Chem. 52 (1974) 355–393.
[28] A. Mohadesi, M.A. Taher, Sens. Actuators B 123 (2007) 733–739.
[29] J.C.B. Fernandes, L.T. Kubota, G.O. Neto, Anal. Chim. Acta 385 (1999) 3–12.
[30] E.A. Hutton, R. Pauliukaitė, S.B. Hocevar, B. Ogorevc, M.R. Smyth, Anal. Chim. Acta 678 (2010) 176–182.
[31] P.A. Kamin, G.S. Wilson, Anal. Chem. 52 (1980) 1198–1205.
[32] C.G. Long, J.D. Gilbertson, G. Vijayaraghavan, K.J. Stevenson, C.J. Pursell, B.D. Chandler, J. Am. Chem. Soc. 12 (2008) 10103–10115.
[33] H.B. Dai, Y. Liang, L.P. Ma, P. Wang, J. Phys. Chem. C 13 (2008) 15886–15892.
[34] L.B. Carvalho Jr., C.J. Lima, P.H. Medeiros, Phytochemistry 20 (1981) 2423–2424.